Disc galaxy modelling with a particle-by-particle made-to-measure method

Jason A. S. Hunt[★] and Daisuke Kawata[★]

Mullard Space Science Laboratory, University College London, Holmbury St. Mary, Dorking, Surrey RH5 6NT, UK

ABSTRACT

We have developed the initial version of a new particle-by-particle adaptation of the made-to-measure (M2M) method, aiming to model the Galactic disc from upcoming Galactic stellar survey data. In our new particle-by-particle M2M, the observables of the target system are compared with those of the model galaxy at the position of the target stars (i.e. particles). The weights of the model particles are changed to reproduce the observables of the target system, and the gravitational potential is automatically adjusted by the changing weights of the particles. This paper demonstrates, as the initial work, that the particle-by-particle M2M can recreate a target disc system created by an *N*-body simulation in a known dark matter potential, with no error in the observables. The radial profiles of the surface density, velocity dispersion in the radial and perpendicular directions, and the rotational velocity of the target disc are all well reproduced from the initial disc model, whose scalelength is different from that of the target disc. We also demonstrate that our M2M can be applied to an incomplete data set and recreate the target disc reasonably well when the observables are restricted to a part of the disc. We discuss our calibration of the model parameters and the importance of regularization.

Key words: Galaxy: structure – galaxies: kinematics and dynamics – galaxies: structure.

1 INTRODUCTION

There is still a gulf between our theoretical galaxy models and the observational data, that must be bridged before we can have a fully dynamical model of the Milky Way which is consistent with its observed properties. The major developments have been localized to certain regions of the Milky Way and the structure of many other regions of the Milky Way remains largely uncertain.

For the last two decades, Galactic astronomy has been relying on *Hipparcos* data (e.g. Perryman et al. 1997). However, new space-based astrometry missions are going ahead in the near future, and ground-based surveys, e.g. PanStaars, (e.g. Kaiser et al. 2010), VISTA (Visible and Infrared Survey Telescope for Astronomy; e.g. Minniti et al. 2009), LSST (Large Synoptic Survey Telescope; e.g. Ivezić et al. 2008), SEGUE (Sloan Extension for Galactic Understanding and Exploration; e.g. Yanny et al. 2009), APOGEE (Apache Point Observatory Galactic Evolution Experiment; e.g. Allende Prieto et al. 2008) and RAVE (e.g. Steinmetz et al. 2006), will add significant value to these missions, which will expand our knowledge of the Milky Way. The next space-based surveys are *Nano-JASMINE* and European Space Agency's cornerstone mission, *Gaia*. *Nano-JASMINE* is a demonstration mission, but it will likely improve on *Hipparcos*' proper motions. *Gaia* is expected to launch in 2013 and will operate for

five years, with a possible one or two year extension. *Gaia* will provide an unprecedentedly large amount of information with which to build a more accurate model of the Milky Way.

Constructing accurate models of the Milky Way is important for allowing us to understand and compensate for observational bias, which are present in all existing Galactic surveys due to dust, gas and our location within the disc. They also allow us to tie together data from different surveys, assembling them into a single model. There are three different types of galaxy model. Mass models only describe the density distribution and the galactic potential (e.g. Klypin, Zhao & Somerville 2002). Kinematic models specify the density and velocity distributions, but lack the constraint that the model must be in a steady state in the galactic potential (e.g. Robin et al. 2004). A model which also satisfies this criterion is known as a dynamical model (e.g. Widrow, Pym & Dubinski 2008). There are arguably five different types of dynamical galaxy model, although sometimes where the line of distinction is drawn can be ambiguous.

Moment-based methods find solutions of the Jeans equation that best fit the observed moments and minimize χ^2 (e.g. Young 1980; Binney, Davies & Illingworth 1990; Magorrian & Binney 1994; Magorrian 1995; Cappellari 2008; Cappellari et al. 2009). The main drawback of this method is that there is no guarantee that there will be a positive distribution function with the required velocity moments. It is also usually restricted to spherically symmetric models as the symmetry allows simplified assumptions to be made. Distribution function based methods fit the distribution function $f(\boldsymbol{r}, \boldsymbol{v})$ to

[★] E-mail: jash2@mssl.ucl.ac.uk

the data directly. The methods have been applied to spherical or integrable systems (e.g. Dejonghe 1984; Bishop 1987; Gerhard 1991; Hunter & Qian 1993; Merritt & Tremblay 1994; Kuijken 1995; Merritt 1996; De Bruyne, Leeuwin & Dejonghe 2000). Perturbation theory can be used to extend the method to near integrable potentials (e.g. Matthias & Gerhard 1999; Binney 2010). Schwarzschild's method works by computing a large number of orbits evolved over many orbital periods in a fixed potential. Information is collected in an orbit library, and it is weighted to produce the best fit to the target model (e.g. Schwarzschild 1979, 1993; Cretton et al. 1999; Gebhardt et al. 2003; Krajnović et al. 2005; Cappellari et al. 2006; Thomas et al. 2009). This method has the advantage of not requiring the distribution function or the other integrals of motion, and rarely, the distribution function may even be recovered (Häfner et al. 2000). This method is not restricted by symmetry, but due to complexity it is usually only used for axisymmetric models. Recently, van den Bosch et al. (2008) have developed a triaxial Schwarzschild method and applied it to NGC 4365. Torus methods are very similar to orbit-based methods, and are often labelled within the same category. The key difference between torus modelling and orbit-based modelling is that while in orbit-based modelling, the orbits are time series of phase space points, in torus modelling, these are replaced by orbital tori (e.g. Binney 2012a,b; McMillan & Binney 2012). For a more detailed explanation and a list of advantages of torus methods over orbit methods, see Binney & McMillan (2011). Finally *N*-body models, which are the simplest to construct, are based on gravitational attraction between '*N*' bodies and can be collisional or collisionless. The key assumption of stellar dynamics in the Galaxy is that these stellar systems are collisionless; hence, collisionless *N*-body models are good approximations for galactic dynamics (e.g. Dehnen & Read 2011).

We will demonstrate an *N*-body method that allows us to recover a model of the desired galaxy, with some flexibility on the initial conditions. Our method is based upon the original made-to-measure (M2M) method by Syer & Tremaine (1996), which is capable of constructing *N*-body equilibrium systems by maximizing a linear combination of the entropy, and minimizing χ^2, the mean-square deviation between the observables and the model. The M2M algorithm has been improved upon by de Lorenzi et al. (2007), Dehnen (2009), Long & Mao (2010) and Morganti & Gerhard (2012) and has been used for a variety of tasks, as detailed below. Bissantz, Debattista & Gerhard (2004) apply the M2M algorithm from Syer & Tremaine (1996) to the Milky Way for the first time, and create a stellar dynamical model of the Milky Way's barred bulge. The model is constrained however by a previously constructed model of the Milky Way from Bissantz & Gerhard (2002), so this new model will be biased towards any inaccuracies from this previous model. The next generation of Milky Way model should be built directly from observational data of the Milky Way, and flexible enough for fitting heterogeneous data.

NMAGIC, developed by de Lorenzi et al. (2007), is the first algorithm to improve upon the initial M2M algorithm by adding the ability to include observational errors in the constraints. This is an important step forward as it allows real observational data to be used as constraints. NMAGIC was also the first M2M algorithm to use velocity constraints, in the form of line-of-sight spectra. NMAGIC has now been applied to several observed galaxies (e.g. de Lorenzi et al. 2008, 2009; Das et al. 2011). Morganti & Gerhard (2012) also made a recent improvement to the field of M2M modelling, by developing moving prior regularization (MPR) which can replace the global weight entropy regularization. Morganti & Gerhard (2012) show that MPR is beneficial to accuracy and smoothness in phase

space distributions, and in some circumstances can converge to a unique solution, independent of the choice of the initial model. To examine M2M's performance against previous methods, Long & Mao (2012) have performed a direct comparison between M2M and the better known Schwarzschild method with regard to calculating the mass-to-light ratios of several elliptical and lenticular galaxies.

These previous M2M algorithms use a distribution function or binned density distribution. However, the data that *Gaia* and the related surveys return will be in the form of individual stellar data. Therefore, we have designed a particle-by-particle M2M algorithm that compares the observables at the location of each star (or the target particle) with the model observables at the same locations, and adjusts the weights in the same fashion as the original algorithm from Syer & Tremaine (1996). In this paper, we present proof of concept of the particle-by-particle M2M by recreating disc galaxies, generated with a Tree *N*-Body code, GCD+ (Kawata & Gibson 2003). Our algorithm uses a self-consistent potential, which evolves over time along with the particle weights. We also show a model constructed from a partial target data set, demonstrating that the observables of the target galaxy do not have to cover the whole galaxy for M2M to work. This is the first step towards the real observational data from Galactic surveys, where the information will be provided for a limited region of the sky, with a more complicated selection function due to the dust extinction, crowding and stellar populations. The paper is organized as follows. Section 2 describes the traditional M2M method and Section 3 describes the methods behind our particle-based adaptation. Section 4 shows the performance of the particle-by-particle M2M for recreating the target disc system. In Section 5 we discuss the accomplishments of this paper, and describe the next stages of our work.

2 THE M2M ALGORITHM

In this section, we will give a brief description of the M2M algorithm as detailed in Syer & Tremaine (1996), de Lorenzi et al. (2007) and Long & Mao (2010), which forms the base for our work. The M2M algorithm works by calculating observable properties (observables hereafter) from the model and the target, and then adapting particle weights such that the properties of the model reproduce those of the target. The target can be in the form of a distribution function, an existing simulation or real observational data. The model is always an *N*-body system.

The observables of the target system are described by

$$Y_j = \int K_j(z) f(z) \, d^6 z, \qquad (1)$$

where *j* represents each individual observable, $z = (r, v)$ are the phase space coordinates, $f(z)$ is the distribution function of the target galaxy and K_j is a known kernel. Observables can come in many forms, including surface or volume densities, surface brightness and line-of-sight kinematics. The corresponding observable for the model takes the form

$$y_j = \sum_{i=1}^{N} w_i K_j[\mathbf{z}_i(t)], \qquad (2)$$

where w_i are the particle weights and $\mathbf{z}_i$ are the phase space coordinates of the model's *i*th particle. We then calculate the difference in the observables of the target and the model,

$$\Delta_j = \frac{y_j(t) - Y_j}{Y_j}. \qquad (3)$$

We then use this Δ_j to determine the so called force of change with the equation

$$\frac{d}{dt} w_i(t) = -\epsilon w_i(t) \sum_j \frac{K_j[\mathbf{z}_i(t)]}{Z_j} \Delta_j(t), \qquad (4)$$

where Z_j so far is an arbitrary constant, and the factor K_i/Z_j can be thought of as the degree to which the ith particle contributes to the jth observable. ϵ is a parameter enabling us to control the rate of change. The linear dependence of equation (4) upon w_i, coupled with the provision that a small enough ϵ is used, ensures that the weights do not become negative. Syer & Tremaine (1996) show a proof of convergence for equation (4) providing that the system starts close to the target.

If $N > J$, i.e. the number of the model particles, N, greatly exceeds the quantity of available constraints, J, the differential equation (4) is ill conditioned. Syer & Tremaine (1996) suggest removing this ill conditioning by introducing entropy, by maximizing the function

$$F = \mu S - \frac{1}{2}\chi^2, \qquad (5)$$

where

$$\chi^2 = \sum_j \Delta_j^2, \qquad (6)$$

and μ is a parameter to control the regularization. The entropy is given by

$$S = -\sum_i w_i \ln\left(\frac{w_i}{\hat{w}_i}\right), \qquad (7)$$

where $\hat{w}_i$ are the priors, a pre-determined set of weights, normally identical to each other such that $\hat{w}_i = M/N$, where M is the total mass of the system and N is the number of particles. The system can be normalized (de Lorenzi et al. 2007) such that

$$\sum_{i=1}^{N} w_i = 1. \qquad (8)$$

This is useful if the total mass of the target system is one of the constraints. We do not impose this restriction as we wish to be able to create a system with a different total mass from the initial model.

Once the new entropy term is introduced to the force of change, equation (4) is replaced by

$$\frac{d}{dt} w_i(t) = -\epsilon w_i(t) \left[\sum_j \frac{K_j[\mathbf{z}_i(t)]}{Y_j} \Delta_j(t) - \mu \frac{\delta S}{\delta w_i}(t) \right], \qquad (9)$$

or

$$\frac{d}{dt} w_i(t) = -\epsilon w_i(t) \left[\sum_j \frac{K_j[\mathbf{z}_i(t)]}{Y_j} \Delta_j(t) + \mu \left(\ln\left(\frac{w_i(t)}{\hat{w}_i}\right) + 1 \right) \right], \qquad (10)$$

for the most complete form. Note that Z_j has been replaced by Y_j due to the maximization of equation (5).

It is shown in Syer & Tremaine (1996) and de Lorenzi et al. (2007) that fluctuations in equation (3) may be reduced by employing temporal smoothing, effectively boosting N without drastically increasing computation time. This is achieved by replacing $\Delta_j(t)$ in equation (4) with $\tilde{\Delta}_j(t)$, where

$$\tilde{\Delta}_j(t) = \alpha \int_0^\infty \Delta_j(t-\tau) e^{-\alpha\tau} d\tau, \qquad (11)$$

with α being small and positive. This $\tilde{\Delta}_j(t)$ can be calculated from the differential equation

$$\frac{d\tilde{\Delta}(t)}{dt} = \alpha(\Delta - \tilde{\Delta}). \qquad (12)$$

This temporal smoothing effectively increases the number of particles from N to

$$N_{\text{eff}} = N \frac{t_{\frac{1}{2}}}{\Delta t}, \qquad (13)$$

where Δt is the length of the time step and $t_{1/2} = (\ln 2)/\alpha$ is the half life of the ghost particles. Syer & Tremaine (1996) show that excessive temporal smoothing is undesirable, and should be limited to $\alpha \geq 2\epsilon$.

The parameters ϵ, μ and α must be determined via parameter search. We will discuss our choice of these parameters in Section 3.4.

3 PARTICLE-BY-PARTICLE M2M

This section describes our original adaptation to the M2M algorithm. The majority of the methodology remains the same as described in Section 2, with the most substantial difference involving the smoothed particle hydrodynamics (SPH) kernel (e.g. Gingold & Monaghan 1977; Lucy 1977), which will be described in Section 3.1. Syer & Tremaine (1996) used a kernel where they divide the coordinate space into bins. For example, for the density at the jth bin with volume V_j, the kernel, $K_j(\mathbf{r}_i)$, is set to be M_{tot}/V_j if $\mathbf{r}_i$ is within the jth bin, where M_{tot} is the total mass of the system and equation (8) is satisfied. If $\mathbf{r}_i$ is outside the jth bin, $K_j(\mathbf{r}_i) = 0$. Because $K_j(\mathbf{r}_1)$ and $K_j(\mathbf{r}_2)$ are the same if $\mathbf{r}_1$ and $\mathbf{r}_2$ are in the same bin, this limits the resolution to the bin size. However, as mentioned in Section 1, our ultimate target is the Milky Way, and the observables are not binned data, but the position and velocity of the individual stars which are distributed rather randomly. To maximize the available constraints, we evaluate the observables at the position of each star and compare them with the N-body model, i.e. in a particle-by-particle fashion. To this end, we introduce a kernel often used in SPH, $W(r, h)$, which is a spherically symmetric spline function given by

$$W(r, h) = \frac{8}{\pi h^3}$$
$$\times \begin{cases} 1 - 6(r/h)^2 + 6(r/h)^3 & \text{if } 0 \leq r/h \leq 1/2, \\ 2[1 - (r/h)]^3 & \text{if } 1/2 \leq r/h \leq 1, \\ 0 & \text{otherwise} \end{cases} \qquad (14)$$

as shown in Monaghan & Lattanzio (1985), where $r = |\mathbf{r}_i - \mathbf{r}_j|$. Note that in our particle-by-particle M2M the kernel, $W(r, h)$, does not explicitly include the total mass, M_{tot}, because we wish to eventually apply it to the Milky Way, whose mass is unknown. Therefore, the SPH kernel in equation (14) is not equivalent to the M2M kernel, K_j, in Section 2.

Below, we describe our particle-by-particle M2M, considering that the target system is an N-body system whose particle position and velocity are known without any error. Of course in the real data of the Galaxy, there are complicated observational errors and selection functions, which often depend on stellar population and dust extinction. In this paper, we ignore these and consider an idealized system for a target. As described in Section 1, the aim of this paper is to demonstrate how our new M2M works and the

potential of future application to the Galactic disc. We below assume that the target system consists of a single population, which we shall refer to as particles, and whose position and velocity are known without errors.

3.1 Method

We use the kernel of equation (14) to calculate the density at the target particle locations, r_j, of both the target and the M2M model. Hereafter, we replace the particle weights, w_i, with their masses m_i due to our adoption of self-gravity in the particle-by-particle M2M. For example, the density of the target at r_j is evaluated by

$$\rho_{t,j} = \sum_{k=1}^{N} m_{t,k} W(r_{kj}, h_j), \tag{15}$$

where $m_{t,k}$ is the mass of the target particle, $r_{kj} = | r_k - r_j |$ and h_j is the smoothing length determined by

$$h_j = \eta \left(\frac{m_{t,j}}{\rho_{t,j}} \right)^{1/3}, \tag{16}$$

where η is a parameter and we have set $\eta = 3$. In SPH simulations, a value of η between 2 and 3 is often used, and we employ the relatively higher value to maximize the smoothness. The solution of equation (16) is calculated iteratively until the relative change between two iterations is smaller than 10^{-3} (Price & Monaghan 2007). Similarly,

$$\rho_j = \sum_{i=1}^{N} m_i W(r_{ij}, h_j), \tag{17}$$

from the model particles. The target density $\rho_{t,j}$ is calculated only once at the beginning of the M2M simulation, and the model density ρ_j is recalculated at every time step.

For velocity constraints, we define the following form of the observables, using the same kernel. For example for radial velocity

$$\delta v_{t,r,j} = \sum_{k=1}^{N} (v_{t,r,k} - v_{t,r,j}) m_{t,k} W(r_{kj}, h_j), \tag{18}$$

where $v_{t,r,k}$ is the radial velocity of the kth target particle and $v_{t,r,j} = (v_{t,x,j} x_{t,j} + v_{t,y,j} y_{t,j})/(x_{t,j}^2 + y_{t,j}^2)^{1/2}$ is the radial velocity of the target system. Equation (18) represents the weighted mean of the relative velocities of the target particles within h_j of the target particle j.

$$\delta v_{r,j} = \sum_{i=1}^{N} (v_{r,i} - v_{t,r,j}) m_i W(r_{ij}, h_j) \tag{19}$$

is similarly calculated from the model particles. The same format is applied for the vertical and rotational velocities.

We then describe the difference in the observables, i.e. equation (3). For density

$$\Delta_{\rho_j} = \frac{\rho_j(t) - \rho_{t,j}}{\rho_{t,j}}. \tag{20}$$

For velocity, we normalized them by the target density because of the density dependence introduced in equations (18) and (19), and therefore for the radial case

$$\Delta_v = \frac{\delta v_{r,j}(t) - \delta v_{t,r,j}}{\sigma_{v_r} \rho_{t,j}}. \tag{21}$$

Note that σ is not an observational error, but just a normalization constant which we have arbitrarily set to $\sigma_{v_r} = \sigma_{v_z} = \sigma_{v_{rot}} = 10 \text{ km s}^{-1}$ in our demonstration in Section 4.

Because Δ_{ρ_j} and Δ_{v_j} are normalized differently, we modified their contribution to the force of change by introducing a new parameter ζ such that for our simulations, equation (10) becomes, with smoothed $\tilde{\Delta}$ by equation (12),

$$\frac{d}{dt} m_i(t) = - \epsilon m_i(t) \left[M \sum_j \frac{W(r_{ij}, h_j)}{\rho_{t,j}} \tilde{\Delta}_{j,\rho}(t) \right.$$

$$+ \zeta M \left(\xi_r \sum_j \frac{W(r_{ij}, h_j)}{\sigma_{v_r} \rho_{t,j}} (v_{r,i} - v_{t,r,j}) \tilde{\Delta}_{v_r,j}(t) \right.$$

$$+ \xi_z \sum_j \frac{W(r_{ij}, h_j)}{\sigma_{v_z} \rho_{t,j}} (v_{z,i} - v_{t,z,j}) \tilde{\Delta}_{v_z,j}(t)$$

$$\left. + \xi_{rot} \sum_j \frac{W(r_{ij}, h_j)}{\sigma_{v_{rot}} \rho_{t,j}} (v_{rot,i} - v_{t,rot,j}) \tilde{\Delta}_{v_{rot},j}(t) \right)$$

$$\left. + \mu \left(\ln \left(\frac{m_i(t)}{\hat{m}_i} \right) + 1 \right) \right], \tag{22}$$

where M is an arbitrary constant mass, which we set as $M = 10^{12} \text{ M}_\odot$ for this paper. Note that in equation (22) the corresponding M2M kernel is $K_j = MW(r, h_j)$, e.g. for density, which is inconsistent with the one used to obtain the observables in equation (17), where $K_j = M_{\text{m,tot}} W(r, h_j)$ and $M_{\text{m,tot}}$ is the total mass of the model particles. However, we accept this inconsistency to apply the method to a system whose total mass is unknown and we allow $M_{\text{m,tot}}(t) = \sum_i m_i(t)$ to freely evolve. Therefore, we introduce the arbitrary constant M in equation (22), and as a result the parameters, such as ϵ, μ and ζ, must be calibrated for the specific system. Fortunately, our ultimate target is only one system, the Milky Way. We hope that we can calibrate the parameters by modelling simulated data before applying the method to the real data. Hence, note that the parameters presented in this paper are specific to the target system in this paper. In future works, we will calibrate the parameters and refine the methods by applying more realistic simulation data.

We use the additional individual parameters ξ_r, ξ_z, ξ_{rot} for the different velocity observables, to allow us to fine tune their contributions to the force of change even further. Similar in spirit to de Lorenzi et al. (2007), we write ϵ as $\epsilon = \epsilon' \epsilon''$ where ϵ'' is given by

$$\epsilon'' = \frac{10}{\max_i \left(M \sum_j \frac{W(r_{ij}, h_j)}{\rho_{j,t}} \tilde{\Delta}_{\rho_j}(t) \right)} \tag{23}$$

for the density observable only.

In the previous works (e.g. Syer & Tremaine 1996; Dehnen 2009; Long & Mao 2010; Morganti & Gerhard 2012), the M2M method is applied to a system in a known fixed potential, i.e. using test particles. de Lorenzi et al. (2007) demonstrate that M2M works with a partially self-consistent potential, in that the potential is calculated every 25 time steps, setting the particle mass $m_i = w_i M_{\text{tot}}$. However, this repeated sudden change of the potential could come with some problems that will be discussed later.

We intend to apply our algorithm to the Milky Way, whose mass distribution is poorly known (e.g. McMillan 2011), and one of the aims of applying the dynamical model is to reconstruct the mass distribution. Therefore, we use a self-consistent disc potential, setting the particle weight, w_i, to the mass, m_i, allowing the disc potential to change along with the model observables and allowing us to recover simultaneously the disc potential along with the mass

and velocity profiles. In this paper, we focus on the disc. We ignore the bulge or halo stars, and assume that the dark matter potential is known for this initial demonstration. Note that the previous studies are mainly focused on elliptical galaxies, i.e. systems dominated by velocity dispersion, but not strongly rotation supported. Recreating a disc galaxy with a self-consistent potential has been attempted once earlier by Deg (2010), who highlights some difficulties with an M2M method that employs self-gravity. He uses a grid to calculate the observables, which makes his method different from ours.

One of the problems arising from using a self-consistent potential as mentioned by Deg (2010) is that the temporal smoothing, which worked well in fixed potential M2M methods, is problematic when used with self-gravity. The temporal smoothing reduces shot noise by averaging Δ_j back along their orbits, which is fine with test particles in a fixed potential because the orbits are fixed. However, in a self-consistent potential, the potential and therefore particle orbits change with time, and thus the temporal smoothing breaks the self-consistency. Therefore, we should be aware that self-gravity M2M models are very sensitive to instabilities, and we see substantial disruption when the smoothing is first turned on. A way to mitigate this damage due to the temporal smoothing is described in Section 3.2. In light of this, we investigated the possibility of running models without temporal smoothing. However, all models had to be substantially underregularized to recover the velocity profiles shown in Section 4, which leads to the continuous fluctuation of the weights, similar to the problems of the underregularization discussed in Section 4.2.

We use a standard Euler method for the integration of the weight change equation and a leapfrog time integrator for advancing the particles. We also use individual time steps for the particles, and only update the masses of particles whose position and velocity are updated within the individual time step. The time step for each particle is determined by

$$dt_i = C_{\mathrm{DYN}} \left(\frac{0.5 h_i}{|d\boldsymbol{v}_i/dt|} \right)^{\frac{1}{2}}, \tag{24}$$

with $C_{\mathrm{DYN}} = 0.2$.

3.2 Target system setup

Our simulated target galaxy consists of a pure stellar disc with no bulge and a static dark matter halo, set up using the method described in Grand, Kawata & Cropper (2012). The dark matter halo density profile is taken from a truncated NFW profile (Navarro, Frenk & White 1997; Rodionov et al. 2009)

$$\rho_{\mathrm{dm}} = \frac{3 H_0^2}{8 \pi G} \frac{\delta_{\mathrm{c}}}{c x (1 + c x)^2} e^{(-x^2)}, \tag{25}$$

where δ_{c} is the characteristic density described by Navarro et al. (1997). The truncation term is introduced in our initial condition generator for a live halo simulation. Although we use a static dark matter halo in this paper, we use the profile of equation (26). Note that the truncation term leads to very little change in the dark matter density profile in the inner region focused on in this paper. The concentration parameter $c = r_{200}/r_{\mathrm{s}}$ and $x = r/r_{200}$, where r_{200} is the radius inside which the mean density of the dark matter sphere is equal to $200 \rho_{\mathrm{crit}}$ and given by

$$r_{200} = 1.63 \times 10^{-2} \left(\frac{M_{200}}{h^{-1} M_{\odot}} \right)^{\frac{1}{3}} h^{-1} \mathrm{kpc}. \tag{26}$$

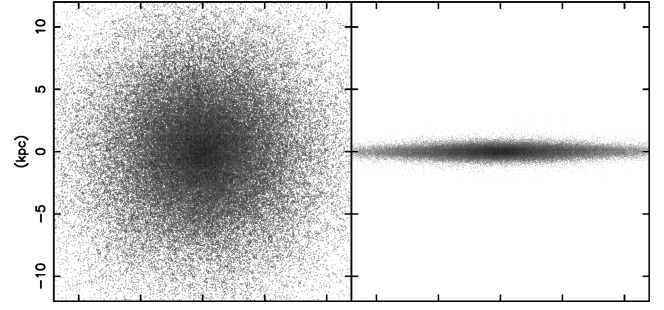We use $M_{200} = 1.75 \times 10^{12} \mathrm{M_{\odot}}, c = 20$ and $H_0 = 71 \mathrm{\ km \ s^{-1} Mpc^{-1}}$.

Figure 1. The end result ($t = 2$ Gyr) of an *N*-body disc galaxy simulation. It had a scalelength of 3 kpc initially. This will be used as the target system as shown in the Section 4. The left- and right-hand panels show the face-on and end-on views, respectively.

The stellar disc is assumed to follow an exponential surface density profile

$$\rho_{\mathrm{d}} = \frac{M_{\mathrm{d}}}{4 \pi z_{\mathrm{d}} R_{\mathrm{d}}^2} \mathrm{sech}^2 \left(\frac{z}{z_{\mathrm{d}}} \right) e^{-R/R_{\mathrm{d}}}, \tag{27}$$

where z_{d} is the scale height of the disc and R_{d} is the scalelength. Our target disc has $z_{\mathrm{d}} = 0.35$ kpc and $R_{\mathrm{d}} = 3.0$ kpc. The disc has a mass of $M_{\mathrm{d}} = 3.0 \times 10^{10} \mathrm{\ M_{\odot}}$ and consists of 10^5 particles, with each particle having a mass of $3.0 \times 10^5 \mathrm{\ M_{\odot}}$. We use the kernel softening suggested by Price & Monaghan (2007). Although Price & Monaghan (2007) suggested adaptive softening length, we use a fixed softening for these simulations for simplicity. Our definition of the softening length $\varepsilon = 1.05$ kpc is about three times larger than the equivalent Plummer softening length. We also use this for the M2M modelling runs. The velocity dispersion for each three-dimensional position of the disc is computed following Springel, Di Matteo & Hernquist (2005) to construct an almost equilibrium condition. We use a high value of the free parameter $f_R = \sigma_R/\sigma_z = 3$, which controls the ratio between the radial and vertical velocity dispersions, to deliberately suppress structure formation and create a smooth, almost axisymmetric disc for this initial test. Our target system is a relatively smooth disc galaxy evolved over 2 Gyr, as shown in Fig. 1, and it is used for all models in Section 4.

We set up the initial conditions of the model disc with the same parameters and method, but use a different scalelength from that of the target galaxy.

3.3 Procedure

The sudden change in potential caused by the changing particle weights induces instabilities and potentially unwanted structure formation. This effect can be reduced by dividing the modelling process into a series of stages, each with a slightly different level of M2M algorithm. This reduces the magnitude of the change in potential at any time. We also set a limit on the maximum change in mass any particle can experience in one time step. We set this limit to 10 percent of that particles mass.

Initially, the model is allowed to relax in a pure self-gravity environment with no M2M constraints for 0.471 Gyr (our *N*-body code time unit). This relaxation period is important, as applying the M2M algorithm before the model has settled generates the aforementioned instabilities. Although our M2M algorithm was still capable of recovering the desired profile, the time-scale needed was drastically increased because the model had to smooth out again before convergence took place if we turned on the M2M without the relaxation period.

Table 1. M2M model parameters.

Model	$R_{d,ini}$ (kpc)	ϵ'	μ	α	ζ	χ^2_ρ	$\chi^2_{v_r}$	$\chi^2_{v_z}$	$\chi^2_{v_{rot}}$	Notes
A	2.0	0.1	5×10^5	0.2	0.05	0.0846	7.291	0.918	6.502	Fiducial
B	2.0	0.1	10^4	0.2	0	0.0831	9.599	1.074	10.873	No velocity
C	2.0	0.1	10^4	0.2	0.05	0.0912	8.275	1.069	7.464	
D	2.0	0.1	10^5	0.2	0.05	0.0875	7.914	1.005	7.087	
E	2.0	0.1	10^6	0.2	0.05	0.0894	7.099	0.893	6.440	
F	2.0	0.1	10^7	0.2	0.05	0.223	9.395	1.130	9.960	
G	2.0	0.1	10^8	0.2	0.05	0.407	17.291	2.107	17.701	
H	5.0	0.1	5×10^5	0.2	0.05	0.100	10.839	1.414	10.394	
I	6.0	0.1	5×10^5	0.2	0.05	0.111	12.381	1.604	12.094	
J	1.5	0.1	5×10^5	0.2	0.05	0.101	7.849	0.972	6.896	
K	2.0	0.1	5×10^5	0.2	0.05	0.0924	7.309	0.911	6.509	Partial data

After this period of relaxation, the M2M algorithm is activated and runs without temporal smoothing for a further 1.413 Gyr, which allows the density and velocity profiles to converge quickly. During this time, the contribution of the velocity constraint is increased linearly from 0 up until our desired ζ. This allows the density profile to converge first. We found this slow increase in the velocity constraints to be important, because if the velocity constraints were introduced simultaneously at full strength, we find the large weight changes induce the sudden potential change mentioned earlier, which is strong enough to disrupt the disc.

Then, after 1.884 Gyr, the temporal smoothing is turned on. When the M2M modelling was run with temporal smoothing from the beginning, the mass profile experienced large oscillations. The modelling then continues in this state for as long as is desired. Our M2M models are run for a period of 10 Gyr.

3.4 Parameter calibration

As discussed in Syer & Tremaine (1996), de Lorenzi et al. (2007), Long & Mao (2010) and Morganti & Gerhard (2012), the choice of parameters is crucial for the success of M2M modelling. In this section, we will discuss our choice of the parameters: ϵ, α, ζ and μ, and how we calibrate these values. Note that these parameters are calibrated for this specific target system. It is likely that we need different calibration for different targets. However, what we learned from the parameter search should be useful for future applications and developments of the improved version.

ϵ provides the balance between the speed of convergence, and the smoothness of the process. In this case, we find that when $\epsilon' > 0.1$, the weights change too rapidly, which induces the sudden potential changes and therefore more instabilities. This leads to a general decrease in the final level of accuracy of both density and velocity profiles. If $\epsilon' \leq 0.1$, convergence can be achieved and the particle weights experience a much smoother evolution. However, if ϵ' is too small, the oscillations generated by the temporal smoothing take too long to damp down, which drastically increases the length of the simulation. In the end, we have chosen $\epsilon' = 0.1$ as a balance between accuracy and simulation time. With more computing power available to us we would consider running a lower value of ϵ. However, if $\epsilon' \ll 0.1$, it is possible that the model will not show any signs of convergence as the weight change is too slow.

The choice of α, which controls the strength of the temporal smoothing, should depend upon the choice of ϵ ($\alpha \geq 2\epsilon$). Note that $\epsilon = \epsilon' \epsilon''$ and ϵ'' is defined by equation (23). We find that our modelling is not sensitive to α and we set $\alpha = 0.2$ in this paper.

ζ (and individual ξ) controls the level of the velocity constraints. It is important to strike a balance between the density and velocity

constraints, because if the level of constraints are unbalanced one will dominate in the change of weight and the other observables will not converge. We can choose a suitable ζ (and/or ξ_r, ξ_z and ξ_{rot}) by comparing the magnitudes of the individual terms of the right-hand side of equation (22). We set ζ such that the contribution of the velocity constraint to the force of change equation is of the same magnitude as, or slightly less than, the density constraints. The individual velocity components may then be fine tuned with ξ_j. For our simulations, we find that the following parameter set works well: $\zeta = 0.05, \xi_r = 1, \xi_z = 10$ and $\xi_{rot} = 1$.

μ controls the strength of the regularization. We discuss the importance of μ in greater detail in Section 4.2. In our fiducial model shown in Section 4 we adopt $\mu = 5 \times 10^5$.

4 PARTICLE-BY-PARTICLE M2M RESULTS

In this section, we present the results from our modelling of our target disc galaxy. We will first show the results for our fiducial model, and then compare it with a model using only density constraints. We ran multiple M2M models with different parameters, which can be seen in Table 1, where $R_{d,ini}$ is the initial scalelength of the model disc. We only use the observables within the radius of 10 kpc.

4.1 Fiducial model

In this section, we present Model A, our fiducial model constructed with the parameters described in Section 3.4 and shown in Table 1. We start from an N-body disc with a scalelength of 2 kpc, recreating the target disc ($R_d = 3$ kpc) with our particle-by-particle M2M, evolving the model for 10 Gyr. Fig. 2 shows the radial profiles of the surface density, radial and tangential velocity dispersion, and the mean rotational velocity. The final profiles of Model A reproduce the profiles of the target system remarkably well. Note that these radial profiles are not direct constraints of the particle-by-particle M2M. Especially, it is rather surprising that the velocity dispersion profiles are recovered. We think that this is because the particle-by-particle M2M forces the model particles to follow the velocity distribution of the target particles. We also have no constraints on the total mass of the disc. Note also that the assumed velocity constant is 10 km s^{-1} in equation (21) yet the velocity profiles are reproduced at a level much less than 10 km s^{-1}. This is not surprising, however, because we have different normalizations for density and velocity, and adjust ζ and ξ to balance their contributions in equation (22) making the choice of σ arbitrary. Therefore, $\sigma_{v_r,t}$ is not indicating an error, but is merely a constant value for normalization. In this paper, we do not include any error. We plan to add more realistic errors in future works. Fig. 3 shows the weight evolution for a selection of particles
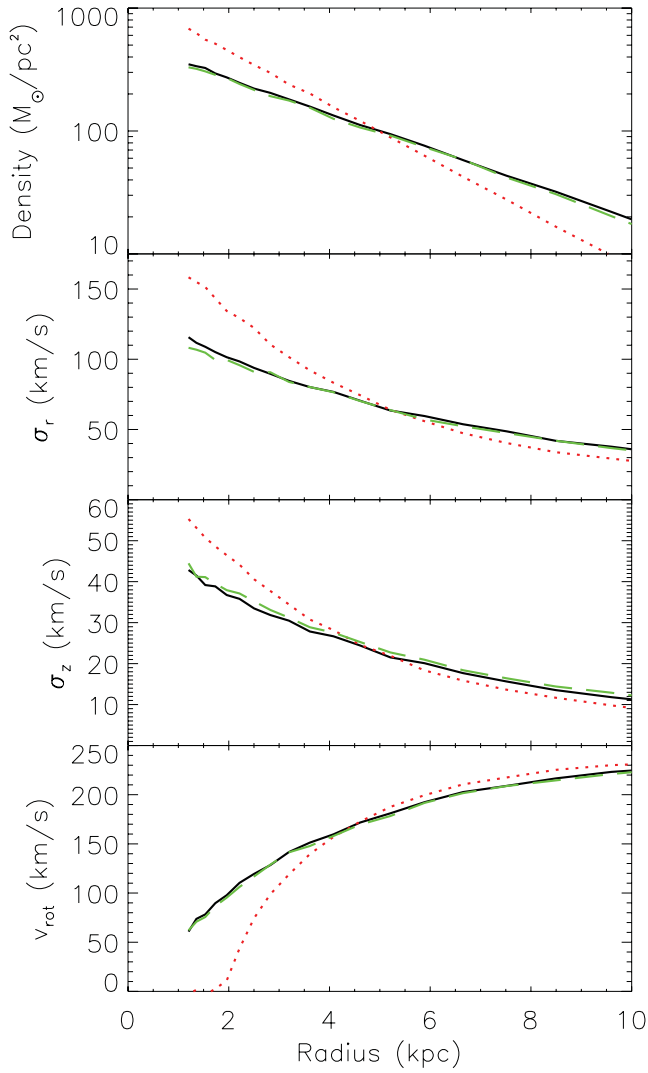
Figure 2. Initial (red dotted), final (green dashed) and target (black solid), density profile (upper), radial velocity dispersion (upper middle), vertical velocity dispersion (lower middle) and rotational velocity (lower) for Model A. The initial model has a scalelength of 2 kpc, the target model has a scalelength of 3 kpc.
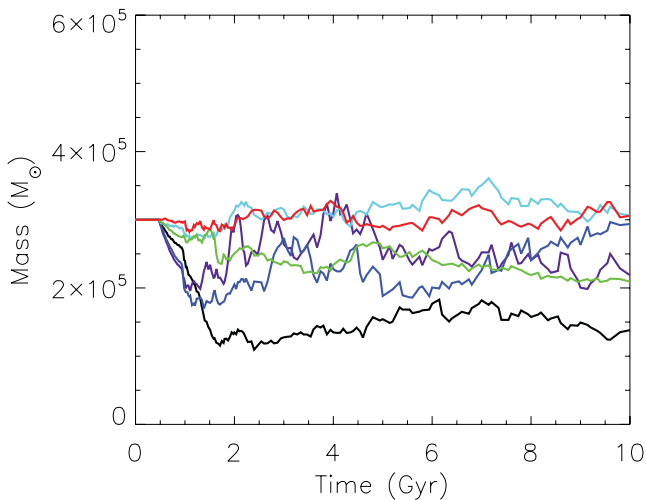

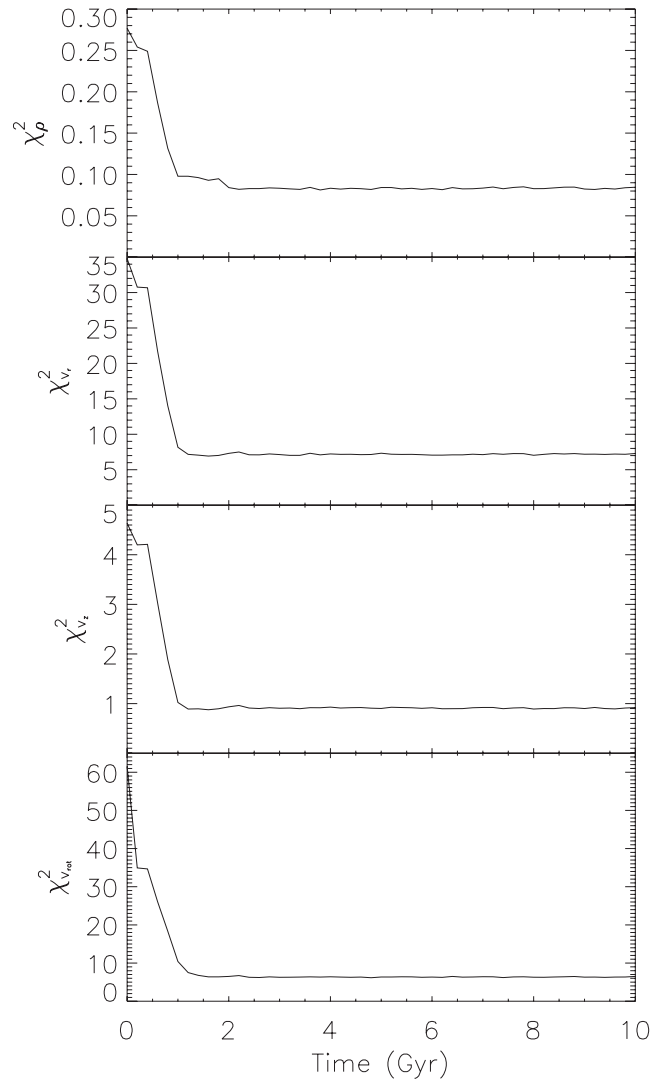**Figure 3.** The weight evolution for a selection of particles from Model A.

Figure 4. Time evolution of χ^2 for density (upper), radial velocity (upper middle), vertical velocity (lower middle) and rotational velocity (lower) for Model A.

from Model A. Weight convergence is adequate, however, it is not as smooth as desired. We find that the particle weight evolution is less smooth for the case where velocity observables have been added. Fig. 4 shows the χ^2 evolution for each of the observables. For all observables we use

$$\chi^2_X = \frac{\sum \Delta^2_X}{N_r}, \tag{28}$$

where Δ_X is equivalent to equations (20), i.e. $X = \rho$, and (21), i.e. $X = v$. This is a slightly unusual definition of χ^2 for the velocity observables. Note that we include only particles within 10 kpc and N_r is the number of target particles satisfying this criteria. In Model A, χ^2 values rapidly decrease until 2 Gyr, from which point there is almost no improvement. The final values of χ^2 are also shown in Table 1.

In comparison we show Model B, with the same initial conditions and target with the velocity constraints turned off. We find that $\mu = 5 \times 10^5$ cause overregularization for this case, and has to be reduced in compensation to $\mu = 10^4$. Fig. 5 shows the density and velocity profiles for Model B. The final model-density profile resembles the target. Due to the lack of velocity constraints, while the velocity
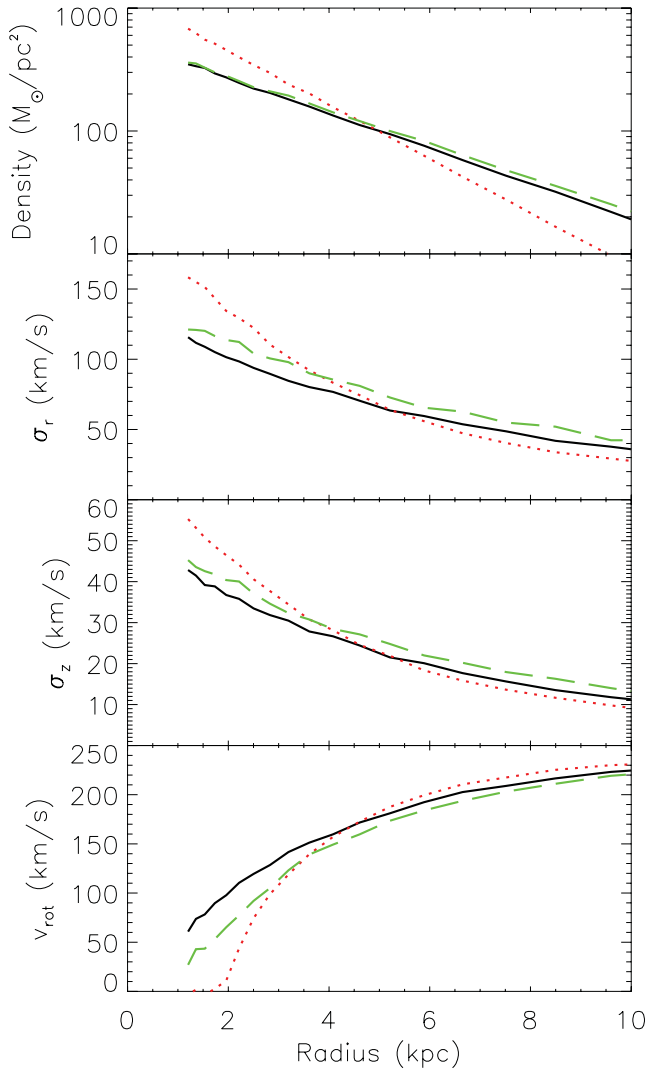
Figure 5. Same as Fig. 2, but for Model B which uses only the density observable as a constraint.

profiles do improve, they do not resemble the target. A comparison between Figs 2 and 5 demonstrates how the velocity constraints improve our reproduction of the dynamical properties of the target.

4.2 Effect of regularization

Similar to the previous studies (e.g. Syer & Tremaine 1996; de Lorenzi et al. 2007; Long & Mao 2010), we also find that careful choice of the value of μ is key to obtain convergence to a good model, and reproduce the given observables. Therefore, we discuss in this section how μ affects the modelling. We performed multiple models with the same initial conditions and parameters as Model A, except the value of μ (see Models C–G in Table 1). Fig. 6 shows the χ^2 for the density and velocity at the final time ($t = 10$ Gyr). The figure demonstrates a slow improvement for the three velocity observables with an increasing μ up until a value of approximately $\mu = 10^6$, above which goodness of fit drops off again. The density observable appreciates a slightly lower value of μ.

Although there is not a vast difference between the final values of χ^2 for $\mu = 10^4$, 10^5, 10^6, Model C with $\mu = 10^4$ is found to be an inappropriate model because of its poor convergence. Fig 7 shows the time evolution of χ^2 in Model C. Fig. 7 shows oscilla-
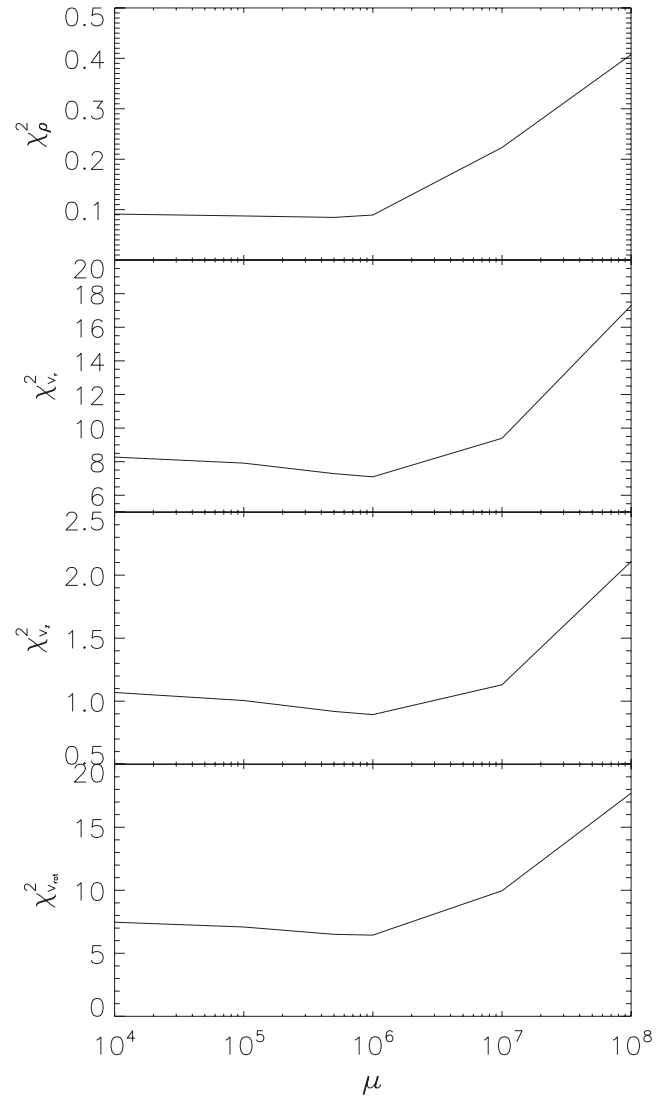
Figure 6. Accuracy of our final M2M model dependent on μ as determined by χ^2 for density (upper), radial velocity (upper middle), vertical velocity (lower middle) and rotational velocity (lower).

tory behaviour. Fig. 8 shows the time evolution of the weight for the particles selected in Fig. 3. Comparison between Figs 3 and 8 demonstrates that $\mu = 10^4$ is too low to suppress the large amplitude of the fluctuations in the particle weights. The weights of the particles keep changing and do not converge. Therefore, we judge that $\mu = 10^4$ is unacceptable for recreating the target system.

Fig. 9 displays the distribution of particle weights at the final time for Models A and C. The histogram shows a wider tail, and lower peak for the underregularized Model C compared to our fiducial Model A. This is expected because a higher μ restricts particles from moving far from the initial mass used as a prior. As a result, Model A shows a narrower distribution and thus a higher peak close to the initial value of w_i. Fig. 9 also demonstrates that $\mu = 10^4$ is less favourable.

If we examine substantial overregularization, i.e. a higher value of μ, it is easy to see the damaging effect on the density and velocity profiles. Fig. 10 shows the profiles from Model G, with $\mu = 10^8$, which shows the significant discrepancy in the density and rotational velocity profiles between the final profiles and the target profiles.
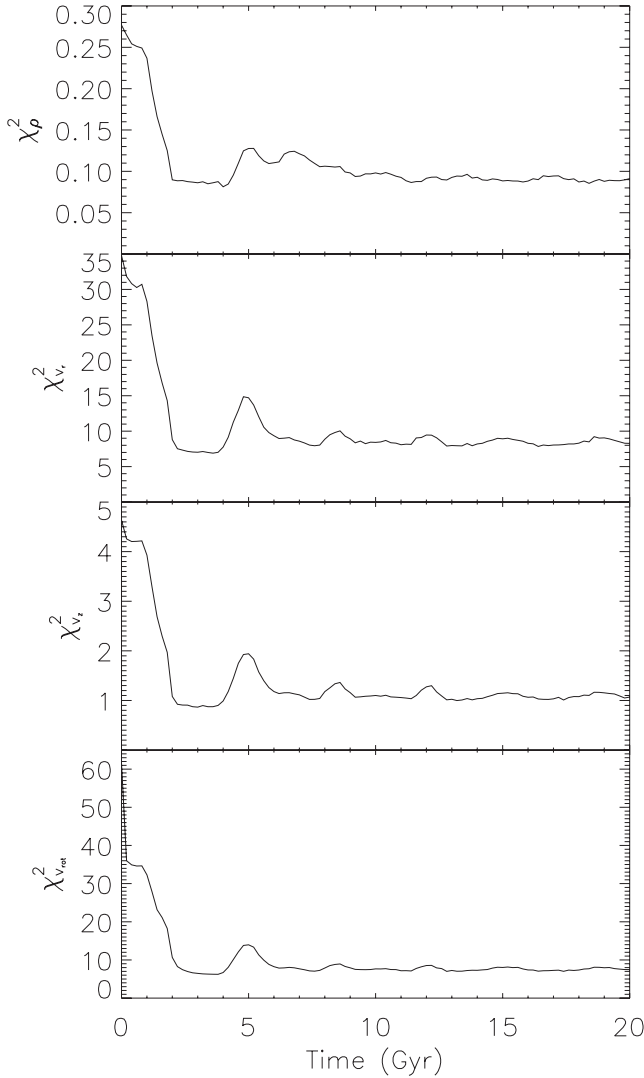
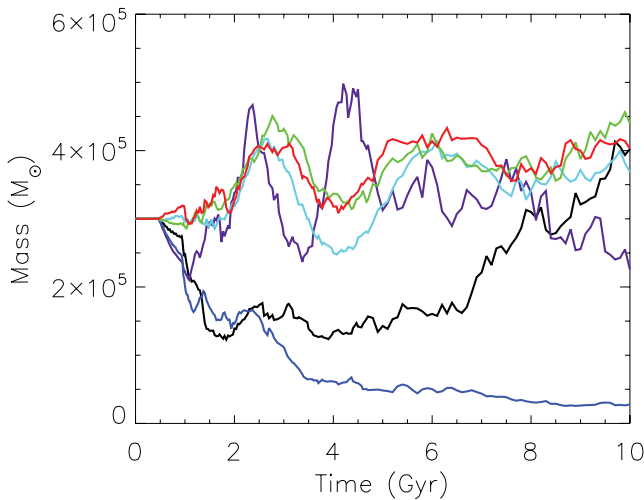**Figure 7.** Same as Fig. 4, but for Model C, with $\mu = 10^4$.

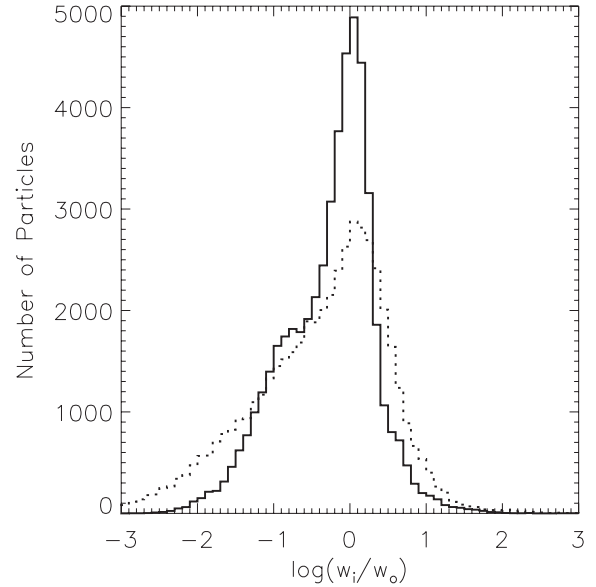**Figure 8.** Same as Fig, 3, but for Model C, with $\mu = 10^4$.

Figure 9. Distribution of particle weights for Model A (solid) and Model C (dotted) at the final time, $t = 10$ Gyr. w_0 indicates the initial particle weights.

The discrepancy in the other two velocity observables is not as substantial. However, it is clearly worse when compared with Fig. 2.

In summary, we found that we required regularization of around $\mu = 10^5 - 10^6$ as a compromise between the goodness of fit, and the smoothness of the χ^2 and particle weight evolution. Both $\mu = 10^7$ and 10^8 show overregularization and the density profiles associated with those values converge to an incorrect profile. $\mu = 10^4$ shows large oscillations in both χ^2 and particle weights, and convergence is not reached. Anything in the range of $\mu = 10^5 - 10^6$ appears appropriate and hence our fiducial model adopts $\mu = 5 \times 10^5$. As can be seen from Table 1, we find underregularization is preferable to overregularization. This is also the case in the previous literature (e.g. de Lorenzi et al. 2008; Morganti & Gerhard 2012) implying this is a generic feature of M2M and not intrinsic to any specific algorithm.

4.3 Different initial conditions

We also tested the algorithm on the same target, using initial discs with a different scalelength, but with the same parameters as Model A. We have already discussed the benefits of tailoring μ to the model, so we were not expecting that these models (Models H and I in Table 1) would recreate their target systems to the same level as Model A. However, for demonstration purposes, we show how the parameter set in Model A works if the initial conditions are different. When we started from a higher initial scalelength (Model H with $R_{d,ini} = 5$ kpc and Model I with $R_{d,ini} = 6$ kpc) we attained a reasonable reproduction of the target. However, the final χ^2 is systematically higher than Model A (see Table 1). Fig. 11 shows the profiles from Model H, which slightly disagree with the targets. This seems to be due to overregularization, and we would need to adjust μ in order to obtain a better model. On the other hand, when we started from a lower initial scalelength (Model J with $R_{d,ini} = 1.5$ kpc, the profiles are shown in Fig. 12), χ^2 was only fractionally worse than the fiducial case Model A (see Table 1). This demonstrates that it is better to set the initial disc with a smaller scalelength. In the application to the real observational data
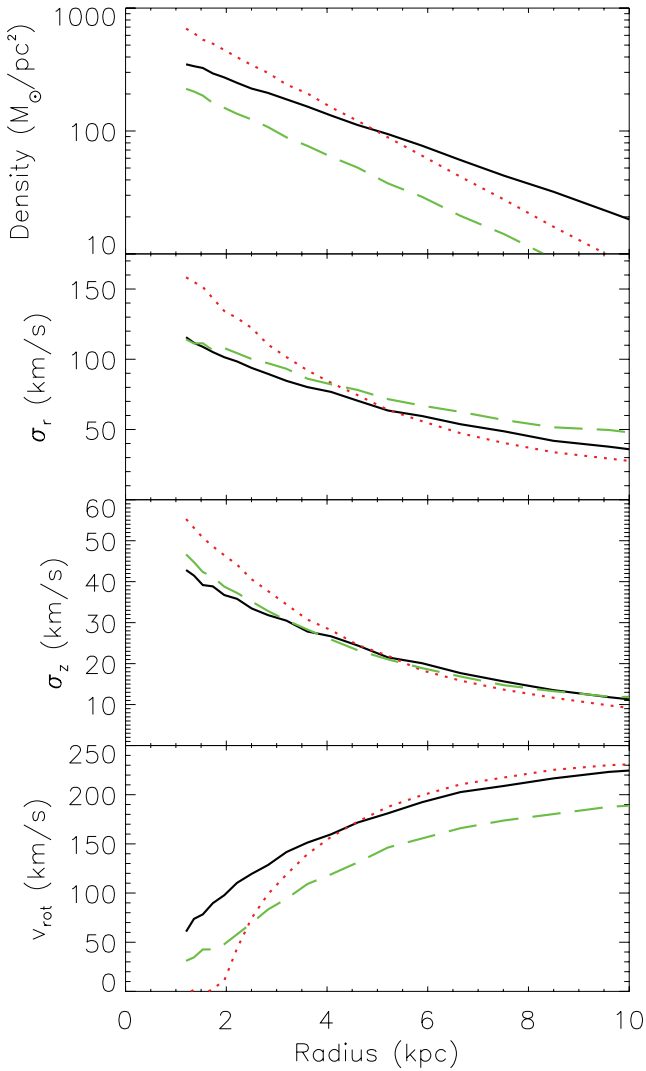
Figure 10. Same as Fig. 2 but for Model G, with $\mu = 10^8$.

Figure 11. Same as Fig. 2, but for Model H, where $R_{\rm d,ini} = 5.0$ kpc.

of the Milky Way, we do not know the right shape of 'the target model'. However, we hope that the further studies with these target galaxies would help us to understand more about how the M2M modelling behaves in different cases, and how we should calibrate the parameters.

4.4 The partial data case

Because our goal is to eventually use our method with *Gaia* data, and *Gaia* will only survey a section of the Galactic disc, it is important to test our algorithm on an incomplete data set (Model K in Table 1). In this paper, a simple selection function is applied for the purpose of demonstration. Remember that our models in the previous sections have used only the data within the radius of 10 kpc from the centre. In this section, we additionally restricted the observables within a 10 kpc sphere around a point in the plane, 8 kpc away from the Galactic Centre.

Fig. 13 shows the final profiles for Model K, which reproduces the target profiles reasonably well. Compared with Fig. 2, Fig. 13 shows only a minor discrepancy to the target profiles, mainly in the outer region. Worse performance in the outer region is unsurprising, as the larger the radii, the smaller percentage of the particles orbits

are spent within the sampled area. Table 1 shows the final values of χ^2, which displays a better value of χ^2 than overregularized models, and similar levels of the goodness of fit to underregularized ones, without the excessive weight oscillations. Model K demonstrates that it is possible to apply our particle-by-particle M2M to a disc galaxy with only a limited selection of data.

5 SUMMARY AND FURTHER WORK

We have developed the initial version of our new particle-by-particle M2M, where the observables are compared at the position of the target particles, and the gravitational potential is automatically adjusted by the weight change of the particles. This paper demonstrates that the particle-by-particle M2M can recreate a target disc system in a known dark matter potential. The radial profiles of the surface density, velocity dispersion in the radial and perpendicular directions, and the rotational velocity of the target disc are all well reproduced from the initial disc model whose scalelength is different from that of the target disc. We find that the regularization parameter, μ, is key to obtaining a reasonable convergence to a satisfactory model. We also demonstrate that our M2M can be applied to an incomplete data set and recreate the target disc reasonably
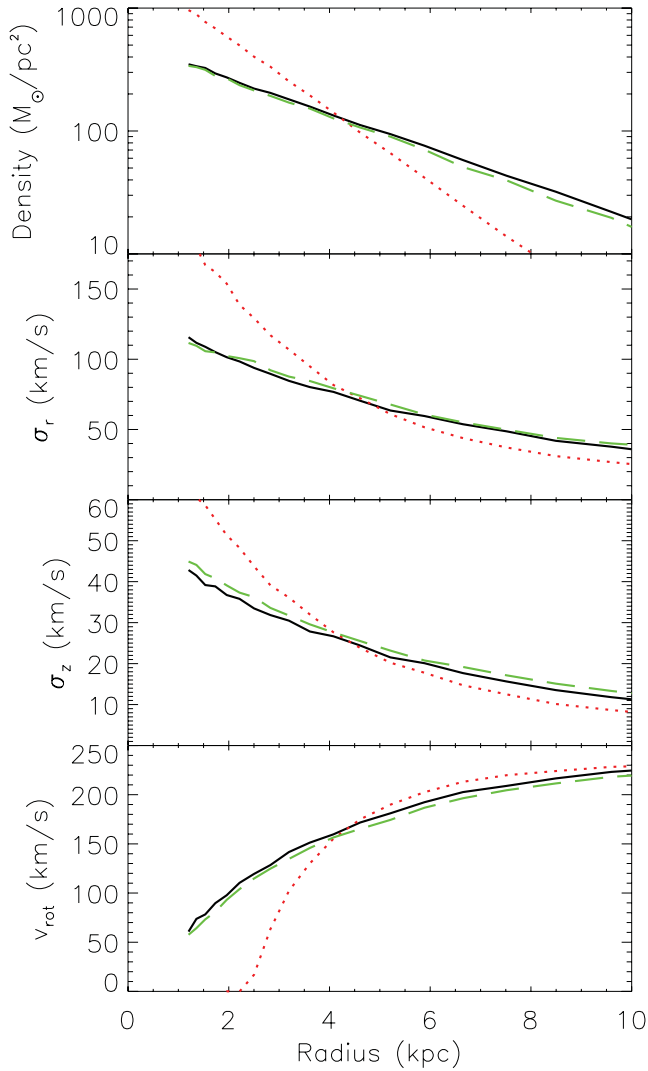
Figure 12. Same as Fig. 2, but for Model J, where $R_{d,ini} = 1.5$ kpc.

Figure 13. Same as Fig. 2, but for Model K, where the observables are calculated only in a sphere of 10 kpc around a point in the plane 8 kpc from the galactic centre.

well when the observables are restricted to within a sphere of radius 10 kpc around a point in the disc plane 8 kpc from the centre.

Admittedly, these applications are simplified cases. Our ultimate goal is to develop the M2M to be applicable to the observational data that *Gaia* and other related Galactic surveys will provide. As discussed above, *Gaia* will produce an unprecedentedly large amount of data of the order of a billion stars, with many dimensions of information. The accuracy of each dimension of information could be quite inhomogeneous, depending on distance, stellar population, and location in the sky due to dust extinction, crowding etc. meaning that the observational selection function is quite complex. There are many challenges before us to develop the M2M for *Gaia*-type data.

We believe that as shown in this paper, it is a good practice for galaxy modelling to attempt to reconstruct galaxy models created by *N*-body simulations, where the full dimensions of the properties are known. Although as an initial attempt, we have taken a disc without any non-axisymmetric structure, and we are trying to apply the method to *N*-body discs with spiral arms and a bar. In the future, we will add more realistic errors and selection functions, to account for dust extinction and crowding. We must then take into account the expected *Gaia* performances, the stellar population
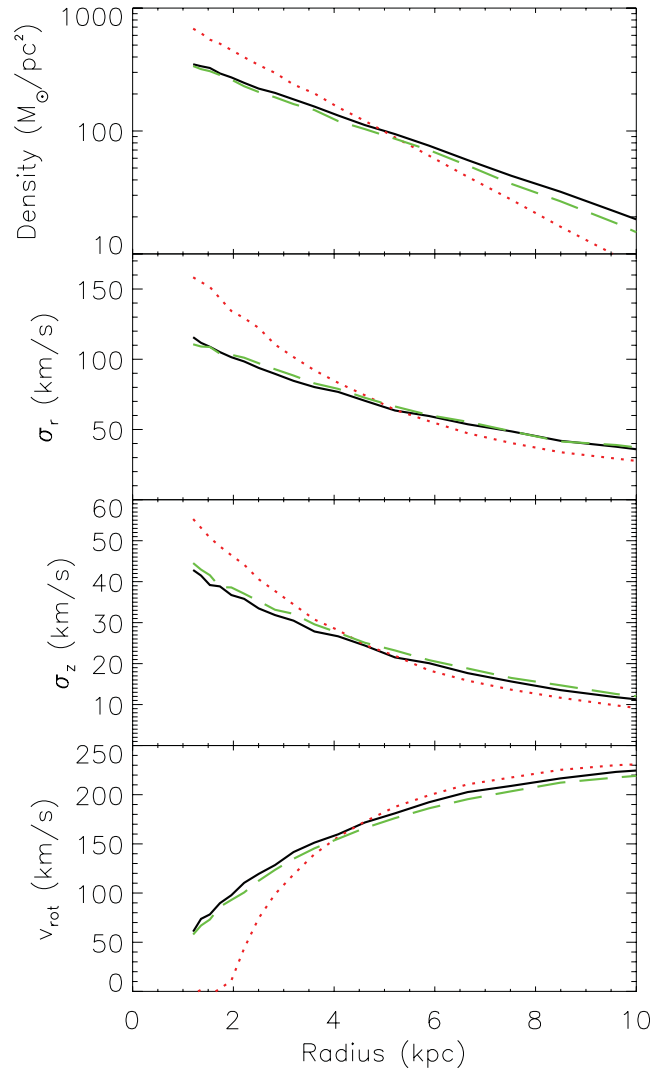
(e.g. Sharma et al. 2011; Pasetto, Chiosi & Kawata 2012) and the three-dimensional dust extinction models (e.g. Drimmel & Spergel 2001; Marshall et al. 2006). We realize that the observables used in this paper are not ideal for such complicated data. We are also investigating other forms of observable and their associated contribution to the force of change, such as the maximum likelihood as applied in de Lorenzi et al. (2008). In this paper, we assume that the dark matter halo potential is known and spherical for simplicity. However, of course we do not know the shape of the dark matter of the Milky Way, and in reality we have to simultaneously explore the different dark matter potential. Another important question is the uniqueness of our M2M solution. Even if the M2M model explains all the observables similarly well. The question remains, what are the 'real' dynamical models for the Milky Way? We hope that many exercises with these 'fake' targets created by *N*-body simulations will be useful to identify the uniqueness of the obtained dynamical model and possible systematic biases.

Encouraged by the success of this paper, we are further improving our particle-by-particle M2M to apply them to the upcoming Galactic observational data, and ultimately construct a dynamical model of the Milky Way.

ACKNOWLEDGEMENTS

REFERENCES

Allende Prieto C. et al., 2008, Astron. Nachr., 329, 1018
Binney J., 2010, MNRAS, 401, 2318
Binney J., 2012a, MNRAS, 426, 1324
Binney J., 2012b, MNRAS, 426, 1328
Binney J., McMillan P., 2011, MNRAS, 413, 1889
Binney J. J., Davies R. L., Illingworth G. D., 1990, ApJ, 361, 78
Bishop J. L., 1987, ApJ, 322, 618
Bissantz N., Gerhard O., 2002, MNRAS, 330, 591
Bissantz N., Debattista V. P., Gerhard O., 2004, ApJ, 601, L155
Cappellari M., 2008, MNRAS, 390, 71
Cappellari M. et al., 2006, MNRAS, 366, 1126
Cappellari M. et al., 2009, ApJ, 704, L34
Cretton N., de Zeeuw P. T., van der Marel R. P., Rix H.-W., 1999, ApJS, 124, 383
Das P., Gerhard O., Mendez R. H., Teodorescu A. M., de Lorenzi F., 2011, MNRAS, 415, 1244
De Bruyne V., Leeuwin F., Dejonghe H., 2000, MNRAS, 311, 297
de Lorenzi F., Debattista V. P., Gerhard O., Sambhus N., 2007, MNRAS, 376, 71
de Lorenzi F., Gerhard O., Saglia R. P., Sambhus N., Debattista V. P., Pannella M., Méndez R. H., 2008, MNRAS, 385, 1729
de Lorenzi F. et al., 2009, MNRAS, 395, 76
Deg N. J., 2010, PhD thesis, Queen's University, Canada
Dehnen W., 2009, MNRAS, 395, 1079
Dehnen W., Read J. I., 2011, Eur. Phys. J. Plus, 126, 55
Dejonghe H., 1984, A&A, 133, 225
Drimmel R., Spergel D. N., 2001, ApJ, 556, 181
Gebhardt K. et al., 2003, ApJ, 583, 92
Gerhard O. E., 1991, MNRAS, 250, 812
Gingold R. A., Monaghan J. J., 1977, MNRAS, 181, 375
Grand R. J. J., Kawata D., Cropper M., 2012, MNRAS, 421, 1529
Häfner R., Evans N. W., Dehnen W., Binney J., 2000, MNRAS, 314, 433
Hunter C., Qian E., 1993, MNRAS, 262, 401
Ivezić Ž. et al., 2008, in   Jin W. J., Platais I., Perryman M. A. C., eds, Proc. IAU Symp. 248, A Giant Step: from Milli- to Micro-arcsecond Astrometry. Cambridge Univ. Press, Cambridge, p. 537
Kaiser N. et al., 2010, Proc. SPIE, 7733, 77330E-1
Kawata D., Gibson B. K., 2003, MNRAS, 340, 908
Klypin A., Zhao H., Somerville R. S., 2002, ApJ, 573, 597
Krajnović D., Cappellari M., Emsellem E., McDermid R. M., de Zeeuw P. T., 2005, MNRAS, 357, 1113
Kuijken K., 1995, ApJ, 446, 194
Long R. J., Mao S., 2010, MNRAS, 405, 301
Long R. J., Mao S., 2012, MNRAS, 421, 2580
Lucy L. B., 1977, AJ, 82, 1013
Magorrian J., 1995, MNRAS, 277, 1185
Magorrian J., Binney J., 1994, MNRAS, 271, 949
Marshall D. J., Robin A. C., Reylé C., Schultheis M., Picaud S., 2006, A&A, 453, 635
Matthias M., Gerhard O., 1999, MNRAS, 310, 879
McMillan P. J., 2011, MNRAS, 414, 2446
McMillan P. J., Binney J., 2012, MNRAS, 419, 2251
Merritt D., 1996, AJ, 112, 1085
Merritt D., Tremblay B., 1994, AJ, 108, 514
Minniti D. et al., 2009, Rev. Mex. Astron. Astrofis., 35, 263
Monaghan J. J., Lattanzio J. C., 1985, A&A, 149, 135
Morganti L., Gerhard O., 2012, MNRAS, 422, 1571
Navarro J. F., Frenk C. S., White S. D. M., 1997, ApJ, 490, 493
Pasetto S., Chiosi C., Kawata D., 2012, A&A, 545, 14
Perryman M. A. C. et al., 1997, A&A, 323, L49
Price D. J., Monaghan J. J., 2007, MNRAS, 374, 1347
Robin A. C., Reylé C., Derrière S., Picaud S., 2004, A&A, 416, 157
Rodionov S. A., Athanassoula E., Sotnikova N. Y., 2009, MNRAS, 392, 904
Schwarzschild M., 1979, ApJ, 232, 236
Schwarzschild M., 1993, ApJ, 409, 563
Sharma S., Bland-Hawthorn J., Johnston K. V., Binney J., 2011, ApJ, 730, 3
Springel V., Di Matteo T., Hernquist L., 2005, MNRAS, 361, 776
Steinmetz M. et al., 2006, AJ, 132, 1645
Syer D., Tremaine S., 1996, MNRAS, 282, 223
Thomas J. et al., 2009, MNRAS, 393, 641
van den Bosch R. C. E., van de Ven G., Verolme E. K., Cappellari M., de Zeeuw P. T., 2008, MNRAS, 385, 647
Widrow L. M., Pym B., Dubinski J., 2008, ApJ, 679, 1239
Yanny B. et al., 2009, AJ, 137, 4377
Young P., 1980, ApJ, 242, 1232

This paper has been typeset from a TEX/LATEX file prepared by the author.